Energy Storage Materials 49 (2022) 58–66

Contents lists available at ScienceDirect

Energy Storage Materials

journal homepage: www.elsevier.com/locate/ensm

A novel organosilicon-type binder for $LiCoO_2$ cathode in Li-ion batteries

Junho Ahn [a], Hyeon-Gyun Im [b], Yongseok Lee [c,d], Dasom Lee [a], Hyekyeong Jang [a], Youngseok Oh [a], Kyeongwoon Chung [a,e], Teahoon Park [a], Moon-Kwang Um [a], Jin Woo Yi [a], Jongsoon Kim [c,d,*], Dong Jun Kang [b,*], Jung-Keun Yoo [a,f,*]

[a] Carbon Composites Department, Composites Research Division, Korea Institute of Materials Science (KIMS), 797 Changwondaero, Changwon, Republic of Korea
[b] Electrical Materials Research Division, Korea Electrotechnology Research Institute (KERI), Changwon, 51543, Republic of Korea
[c] Department of Energy Science, Sungkyunkwan University, Suwon, 16419, Republic of Korea
[d] SKKU Institute of Energy Science and Technology (SIEST), Sungkyunkwan University, Suwon 16419, Republic of Korea
[e] Department of Biofibers and Biomaterials Science, Kyungpook National University, Daegu, 41566, Republic of Korea
[f] Advanced Materials Engineering Division, University of Science and Technology (UST), Daejeon, 34113, Republic of Korea

ARTICLE INFO

Keywords:
High structural stability
Silicon-organic-based binder
Li-ion Batteries
Slot-die coating
First-principles calculation

ABSTRACT

The conventional binder used in LIBs, polyvinylidene fluoride (PVDF), possesses low mechanical ductility and weak affinity to electrode materials and therefore cannot prevent pulverization of the cathode materials or undesirable battery swelling after prolonged cycling. Herein, we introduce a novel organosilicon-type binder (S-binder), composed of siloxane (Si–O–Si), silanol (Si–O–H), and cyclohexene oxide ($C_6H_{10}O$) groups. It is demonstrated that S-binder exhibits the enhanced adhesion to the cathode, high elasticity, and great flexibility compared with PVDF, resulting in exceptionally improved electrochemical performances of $LiCoO_2$. In terms of cyclability, S-binder-applied $LiCoO_2$ electrode with high mass loading of the active material (~8 mg cm^{-2}) exhibits outstanding capacity retention of ~92.0% compared with the initial capacity after 100 cycles. From industrial perspective, simulation of the slot-die coating on S-binder- and PVDF-applied slurries indicates the high competitiveness of S-binder compared with PVDF for the mass-production of $LiCoO_2$ electrode for LIBs.

1. Introduction

Li-ion batteries (LIBs) have received great attention as promising ESSs for not only small electronic devices such as laptops and cellphones but also large-scale applications such as electric vehicles (EVs) [1–2]. Moreover, with the explosive growth of demands for LIBs toward EVs and grid-scale ESSs, not only high energy density but also stable and reliable long-term usage are considered important for LIBs, indicating the significance of creating a stable operation environment for the cathode and anode materials [2–5].

$LiCoO_2$, one of the most promising commercialized cathodes for Li-ion batteries (LIBs), exhibits a high redox potential of ~3.9 V (*vs.* Li^+/Li) and a large theoretical capacity of ~254 mAh g^{-1} [6]. However, $LiCoO_2$ experiences an irreversible O3–O1 phase transition during deintercalation of above 0.5 mol Li^+ at the high voltage region, limiting the available capacity during charge/discharge despite the large theoretical capacity [7]. Recent works have shown that the structural instability of $LiCoO_2$ occurring after Li^+ deintercalation is mainly affected by controlling the surface reaction between particles and electrolyte [8–9]. The reversibly available capacity of $LiCoO_2$ can be increased to ~180 mAh g^{-1} through surface modification [10]. However, most of the reported surface modification methods for $LiCoO_2$ particles are based on coating of the inorganic compounds at the surface of particles [11–12]. During charge/discharge, the inorganic compounds may be fragile because of repeated large expansion and shrinkage of the $LiCoO_2$ particles, resulting in poor cycle performance of $LiCoO_2$ by the structural degradation [13]. Thus, it is important to provide an efficient buffer for the $LiCoO_2$ particles to prevent not only irreversible electrochemical reaction at the surface of particles but also structural degradation after prolonged cycling.

One simple route to achieve an efficient buffer for $LiCoO_2$ cathodes is to use an outstanding binder, one of the principle components of LIBs [14]. Polyvinylidene fluoride (PVDF) has been applied as the suitable binder for the operation conditions in the LIB cell due to the wide electrochemical window and high chemical resistance [15]. However, the intrinsic properties of PVDF, such as low mechanical ductility, weak affinity to electrode materials, and dissolution in organic electrolyte, results in inevitable physical swelling and pulverization of the electrode materials during prolonged cycling, which implies that PVDF cannot be applied as an efficient buffer for the particles to enhance the poor cycle performance of $LiCoO_2$ [16]

* Corresponding authors.
E-mail addresses: jongsoonkim@skku.edu (J. Kim), kangdj@keri.re.kr (D.J. Kang), yoojk@kims.re.kr (J.-K. Yoo).

https://doi.org/10.1016/j.ensm.2022.04.005
Received 9 February 2022; Received in revised form 22 March 2022; Accepted 3 April 2022
Available online 5 April 2022

Herein, it is demonstrated that a novel organosilicon-type binder (S-binder) can exceptionally improve the cycle-performance and power-capability of $LiCoO_2$ compared with PVDF. Organosilicon (or siloxane) materials have excellent chemical/thermal robustness and processability, which are the essential properties of the LIB binder. It was reported that the organic-inorganic-based nanohybrid structures of organosilicon materials exhibit not only the inorganic-like stability but also organic-like processability [17]. Moreover, the hydrolytically synthesized epoxy-siloxane materials consist of the hydroxyl groups that effectively interact with the surface of the oxide-based materials via hydrogen bonding and condensation reaction. Thus, we supposed that the epoxy-siloxane materials can be applied as the novel binder for $LiCoO_2$ cathode to suppress the severe structural change occurred during charge/discharge successfully. Through combined studies using first-principles calculation and various experiments, it was demonstrated that S-binder enables not only strong adhesion to the surface of $LiCoO_2$ particles but also homogenous coating of the particles without self-aggregation of the binder. In particular, S-binder-applied $LiCoO_2$ (S-b-LCO) electrode delivered an outstanding capacity retention of ~92.0% for 100 cycles, whereas the PVDF-applied $LiCoO_2$ (PVDF-LCO) exhibited poor cycle performance with a capacity retention of ~49.8% under the same conditions. Furthermore, S-binder has more merits than PVDF for application in the LIB industry through the simulation of slot-die coating on S-b-LCO and PVDF-LCO slurries.

2. Experimental

2.1. Preparation of $LiCoO_2$

Commercially available solutions of PVDF and CNTs dispersion were purchased from Kureha Co., Ltd. (Japan) and Advanced Nano Products Co., Ltd. (Korea), respectively. NMP was purchased from Daejung Chemical & Materials Co., Ltd. (Korea). $LiCoO_2$ (Monatri Co., Ltd.) was used as received without further processing. All the reagents to synthesize S binder were purchased from Sigma Aldrich (USA) and TCI (Japan) and used without further purification.

2.2. Synthesis of S binder

22.1 g of (2-(3,4-epoxycyclohexyl)ethyl)trimethoxysilane (ECTMS) and 2.1 g of tetraethyl orthosilicate (TEOS) were put into a two-neck flask filled with 50% of NMP solvent and vigorously mixed with magnetic stirrer under room temperature. 2.8 g of ammonium hydroxide solution (28%) was dropwise added into the solution while temperature was elevating to 60°C. After 8 hours of string, highly viscous and clear binder resin (S binder) was obtained. 1 phr of cyclohexyl *p*-toluenesulfonate as a thermal initiator was added into the binder for the subsequent polymerization of epoxy groups. From safe point of view, PVDF binder has a lot of fluoro-groups, which can generate toxic fluoro-gaseous-compounds, however, S-binder does not have. S-binder has organic-inorganic hybrid chemical structure composed of siloxane backbone (inorganic) and cycloaliphatic epoxy moiety (organic), and these components are not hazardous.

2.3. Materials characterization

The rheometer (Anton Paar Physica MCR 302) was utilized to examine composite properties, such as the mixtures with and without active materials, by measuring shear viscosity (shear rate: 1–500 s^{-1}) of the slurry using a parallel plate with a 25-mm diameter and 0.25-mm gap as well as the frequency sweeps at room temperature with decreasing frequency from 100 to 0.1 rad/s (strain 0.5 %). The solution (DMSO-d6 as a solvent) and solid state NMR spectra (13C and 29Si) of the S binder were obtained using a Bruker DRX 300 spectrophotometer (Korea Basic Science Institute). IR spectra of S binder range of 600 to 4000 cm-1 are confirmed to support structure information before and after polymerizations. Surface tension of slurry was measured by Tensiometer (KRÜSS, K100SF-MK2) with Pt plate as a probe for detect their tensions. Contact angle measurements (KRÜSS, DSA100) of slurry are performed by dropping the slurry on Al collector. A Theta Probe AR-XPS System (Busan Center, KBSI, Korea) with ultrahigh vacuum chambers was used to obtain XPS data for the freestanding electrodes. SEM images were observed using a JSM-6700F (JEOL) under an accelerating voltage of 15 kV. The electrodes after treated with cross section polisher using IB-19520CCP (JEOL) under an accelerating voltage of 4 kV were observed to obtain CP-SEM images.

2.4. Fabrications of electrodes and electrochemical characterization

The slurries were prepared by high shear mixing at 3000 rpm for 15 min of electrode materials as specified ratios of $LiCoO_2$ (0.3 kg), CNT dispersion solution (0.6 wt *vs*. LCO), and binder (1.2 wt% *vs*. LCO) solution. Solid contents of S binder in NMP solvents were 50 wt%. The doctor-blade-coated electrode layer on Al foils were dried at 80 °C 2 hours and then dried at 120 °C for 12 h. The mass loading of the electrode layer was approximately ~8 mg/cm^2. The resistances of the high-energy-density electrode (4 cm^2) were measured using a Hioki electrode resistance meter (XF-057) with constant current (10 mA). To calculate active layer and interface resistances of electrodes, the resistances and thickness of Al foil were 2.65×10^{-6} Ω cm^{-1} and 20 μm, respectively. To evaluate the electrochemical performance of the electrodes, coin-cells (2032 coin) consisted of an electrode, a PP separator (Celgard 2400), electrolyte (1 M LiPF6 in EC:DMC (ethylene carbonate:dimethyl carbonate), 1:1 by volume) and a Li counter electrode were assembled in a glove box under highly pure Ar. The area of punched electrodes in cells were 1.538 cm^2. Galvanostatic charge/discharge tests in the voltage range of 3–4.5 V at 25°C were performed at various C rates (C/10, C/2, 1C, 2C, 3C, 4C, 5C and 6C, where 1C corresponds to 150 mA g^{-1}) for $LiCoO_2$. Charge–discharge curves were recorded using a WBCS 3000 battery tester system (WonA Tech). Electrochemical impedance spectroscopic analysis was performed at frequencies of 0.1 MHz to 0.1 Hz with a voltage amplitude of 0.01 V using a ZIVE SP1 electrochemical workstation (WonA Tech). In addition, CV measurements were performed using coin cells in the voltage range of 3–4.5 V at a scan rate of 0.2 mV s^{-1}. GITT measurements of cells at 0.33C and 0.5C delivered under current pulse for 10 minutes at voltage range of 3-4.5 V.

3. Results and discussion

S-binder synthesized through a simple condensation process between tetraethyl orthosilicate (TEOS) and [2-(3,4-epoxycyclohexyl)ethyl]trimethoxysilane formed multi-dimensional molecular networks via hydrogen bonding of cyclohexene oxide ($C_6H_{10}O$) and hydroxyl (-OH) group, enabling the high structural stability and flexibility of S-binder (Fig. 1) [18–19]. Each S-binder unit is also chemically bonded with each other through formation of polyethers by polymerization of epoxide (C–O–C) groups [20]. With the hydrogen bonding and chemical interactions occurring during the polymerization process, S-binder can cover $LiCoO_2$ particles more homogeneously without self-aggregation than PVDF [21]. Thus, it was expected that application of S-binder would enable suppression of the irreversible structural change of $LiCoO_2$ compared with usage of PVDF after repeated charge/discharge cycling.

The improved adhesion of S-binder with $LiCoO_2$ compared with that of PVDF was theoretically investigated using first-principles calculation. Fig. 2 presents a comparison of the theoretical adsorption energies (E_{ads}) and the optimized geometric structures of S-binder, PVDF, and polyacrylic acid (PAA) monomers on the (001) surface of $LiCoO_2$. The E_{ads} values were calculated using the following equation:

$$E_{ads} = E_{LiCoO_2(001)@binder} - (E_{LiCoO_2(001)} + E_{binder}),$$

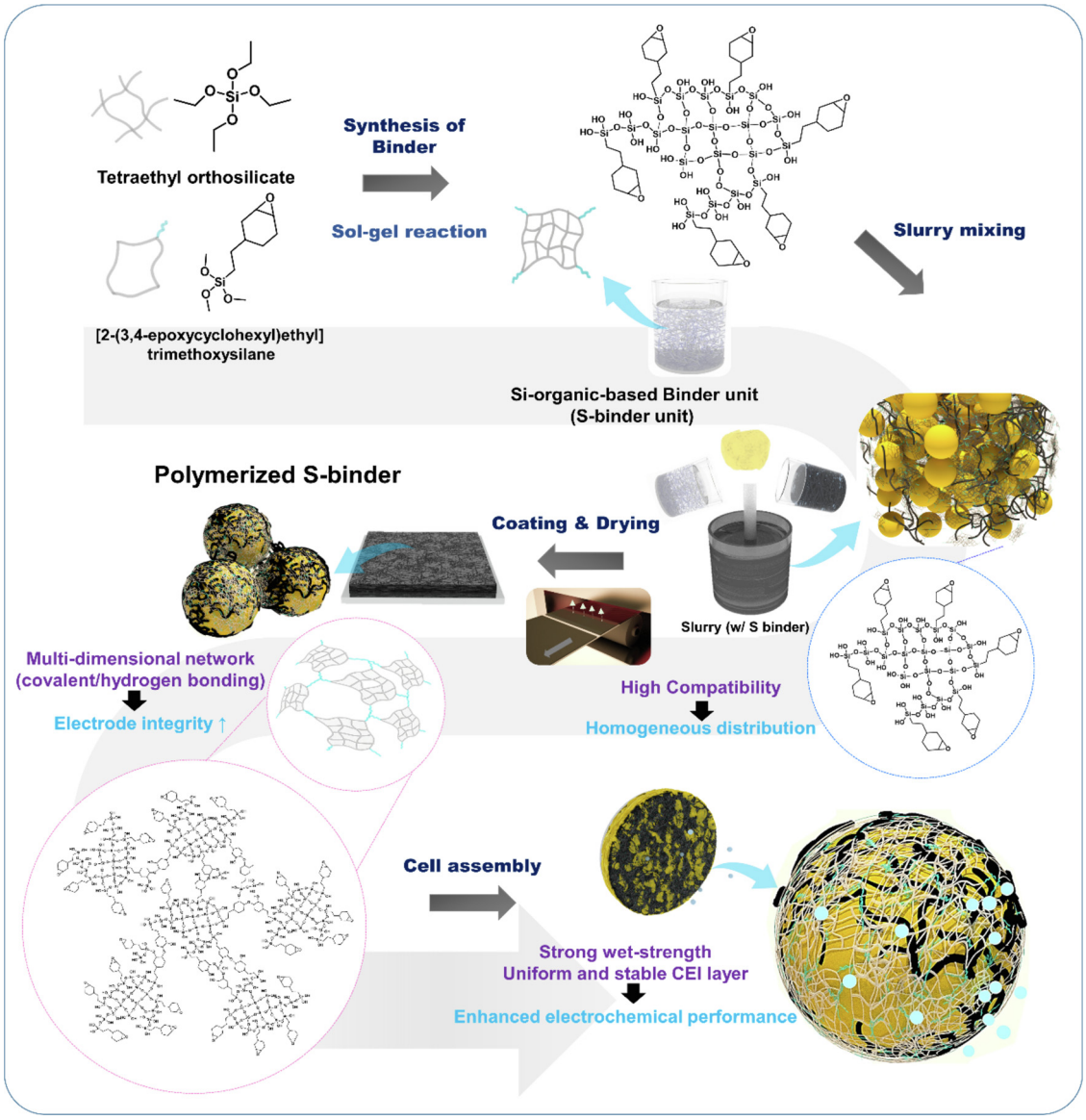

Fig. 1. Illustrations of synthesis process of the S-binder and their operation mechanism during electrode and cell levels.

where $E_{LiCoO2@binder}$ is the total energy of the (001) surface of $LiCoO_2$ that adsorbed the binder, $E_{LiCoO2@binder}$ is the total energy of the pristine (001) surface of $LiCoO_2$, and E_{binder} is the total energy of the binder monomer. It was verified that the adsorption energy of S-binder is −1.451 eV, which is much lower than that of PVDF (−0.157 eV) and PAA (−0.249 eV). These first-principles calculation results imply that S-binder more effectively and strongly adheres to the surface of $LiCoO_2$ than the well-known PVDF and PAA binders for LIBs.

The successful preparation of S-binder was verified through Fourier-transform infrared spectroscopy (FTIR) analyses, confirming the presence of the Si–O–H (1031 cm^{-1}) and Si–O–Si (1076 cm^{-1}) peaks (Fig. S1) [19]. The average molecular weight (Mn) of S-binder solution is ~4170 g mol^{-1}. The ^{29}Si nuclear magnetic resonance (NMR) analyses also indicate successful hydrolysis and condensation (Fig. 3**a**), with evident peak shifts from −41 to −59 and −68 ppm (red line) [22]. In addition, S-binder formed the irreversible gels owing to progress of further chemical reactions, such as sol–gel condensations and ring-opening reactions, under the drying process at 120 °C [20]. We also observed appearance of non-cyclic ether groups and decline of epoxide groups after polymerization of S-binder through ^{13}C-NMR and FTIR analyses (Fig. 3**b** and Fig. S1). Further sol-gel condensations of silanol groups also occurred during the drying step. The peak at −59 ppm that vanished after further curing of S-binder indicates an additional condensation reaction (Fig. 3**b**) [22]

Using scanning electron microscopy (SEM), we compared morphologies and thickness uniformity between the S-b-LCO and PVDF-LCO electrodes. As shown in Fig. 3**c**, there was no noticeable variation in thickness of the S-b-LCO electrode, as a result of the lack of severe aggregation of S-binder with carbon-nanotube (CNT) conductive agent and homogenous distribution of $LiCoO_2$ particles. In contrast, considerably large self-aggregation of PVDF with CNT occurred in the PVDF-LCO electrode, and some $LiCoO_2$ particles were far away from each other, resulting in non-uniformity of thickness in the PVDF-LCO electrode (Fig. 3**d**). Moreover, we prepared the S-b-LCO and the PVDF-LCO electrodes with high mass loading of ~16 mg cm^{-2}. Fig. S2 shows the low-magnified cross-sectional SEM images of the S-b-LCO and the PVDF-LCO electrodes. It was clearly verified that the S-b-LCO electrode exhibits much better uniformity than PVDF-LCO electrode. These results indicate that application of S-binder with high adherence to the surface of $LiCoO_2$ enables high uniformity of the overall morphology and thickness in the S-b-LCO electrode for highly enhanced electrochemical performance of

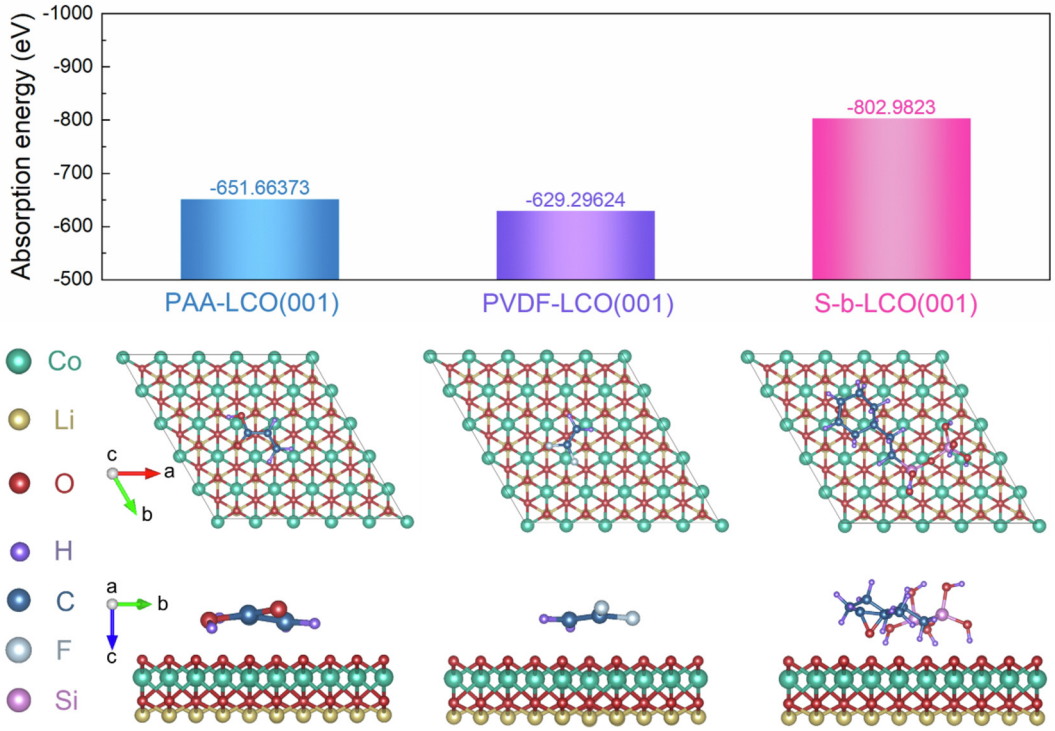

Fig. 2. Theoretical adsorption energies of binders: Comparison of the theoretical adsorption energies (E_{ads}) and the optimized geometric structures of S-binder, PVDF and polyacrylic acid (PAA) monomers on the (001) surface of $LiCoO_2$

$LiCoO_2$. Through X-ray photoelectron spectroscopy (XPS) analyses (Fig. S3), it was verified that peak intensities of Co 2p spectra related to the $LiCoO_2$ phase become smaller through application of S-binder instead of PVDF, which implies that S-binder can cover $LiCoO_2$ particles on the electrode more homogeneously than PVDF, because of the enhanced adhesive properties. The peaks of F 1s and Si 2p spectra were clearly detected in the XPS results for the PVDF-LCO and S-b-LCO electrodes, respectively, indicating that PVDF and S-binder were applied to each electrode. Furthermore, the SEM analyses (Fig. S4) indicate that application of S-binder can result in more homogeneously wrapped $LiCoO_2$ particles by the binder and the conductive carbon, which agrees well with the XPS results.

In addition, it was known that the morphology of the electrode is affected by interaction among the active material, conducting agent, and binder during the slurry-mixing process and the electrode-coating/drying process [21]. Thus, we compared the complex shear modulus and shear viscosity between S-b-LCO and PVDF-LCO slurries. The complex shear modulus $G^*(\omega)$ was quantified using the storage $G'(\omega)$ and loss $G''(\omega)$ shear moduli as $|G^*(\omega)| = [G'(\omega)^2 + G''(\omega)^2]^{0.5}$. Fig. 3**e** shows that the S-b-LCO slurry exhibited a larger complex shear modulus (68.4 Pa) than the PVDF-LCO slurry, indicating the higher elasticity of the S-b-LCO slurry. The enhanced elastic property of the S-b-LCO slurry is attributed to the cross-linking via condensation reaction between silanol functional groups, which results in high surface tension of slurries (Fig. 3e). Generally, the slurry exhibits both the liquid-like viscous property and the solid-like elastic property. Fig. S5a below shows the viscoelastic properties of the PVDF-LCO, S-b-LCO (1.2 wt% S-binder) and S-b-LCO_1 (1.8 wt% S-binder) slurries. It was verified that the S-b-LCO and S-b-LCO_1 slurries deliver larger solid-like elastic property than the PVDF-LCO slurry, which implies that S-binder can provide more strong interaction with the active material and the conductive carbon than PVDF. Especially, we confirmed increased contents of S-binder from 1.2 wt% to 1.8 wt% in the slurry results in increase of the solid-like elastic property. In case of PVDF, on the other hand, we previously reported that the solid-like elastic property is decreased with increase of PVDF contents in the LCO-based slurry. [23]. Since PVDF can play a role of the surfactant in the slurry, more usage of PVDF can strengthen the liquid-like viscous property of the slurry. The principle compositional difference between PVDF and S-binder is the presence or absence of the functional groups. Unlike PVDF, S-binder is composed the diverse functional groups. Thus, by the strong interaction and condensation reaction among the functional groups, increase of S-binder contents in the slurry results in the increase of the solid-like elastic property. Moreover, it was verified that the viscosity of S-b-LCO_1 is higher than that of S-b-LCO in the low shear rate (Fig. S5b), which supports that the solid-like elastic property is strengthened by increase of S-binder contents in the LCO-based slurry. In addition, Table S1 below shows the S-binder applied slurries exhibit larger surface tension than the PVDF-applied slurry. In particular, the surface tension is also increased with more usage of S-binder contents in the slurry, which is connected with the strengthened attraction among S-binder units by increase of the contents. Moreover, the tendency of the contact angle to change are similar with those of the surface-tension to change, which indicates that the contact angle can be enlarged with increase of the S-binder contents by highly strong condensation reaction among the units. The strong condensation reaction of S-binder compared to that of PVDF enables more enhanced elastic property and surface tension of the S-b-LCO slurry than those of the PVDF-LCO slurry. Therefore, application of S-binder enables uniform thickness of the electrode after deposition of the slurry onto the electrode. To confirm the strong cohesiveness of the S-binder compared with PVDF binder, we measured the mechanical property of the PVDF-LCO and S-b-LCO electrodes through the 180° peeling test using universal testing machine (UTM). As shown in Fig. S6, it was verified that the S-b-LCO electrode required higher peeling strength (~11.49 N) than the PVDF-LCO electrode (~8.47 N), which indicates that S-binder exhibits the superior cohesiveness compared to PVDF binder. Moreover, increased elasticity and high-shear thinning behavior achieved by application of S-binder can result in enhanced dispersion of the active materials and high uniformity in the S-b-LCO electrode, as explained in the SEM analyses (Fig. 3**f**).

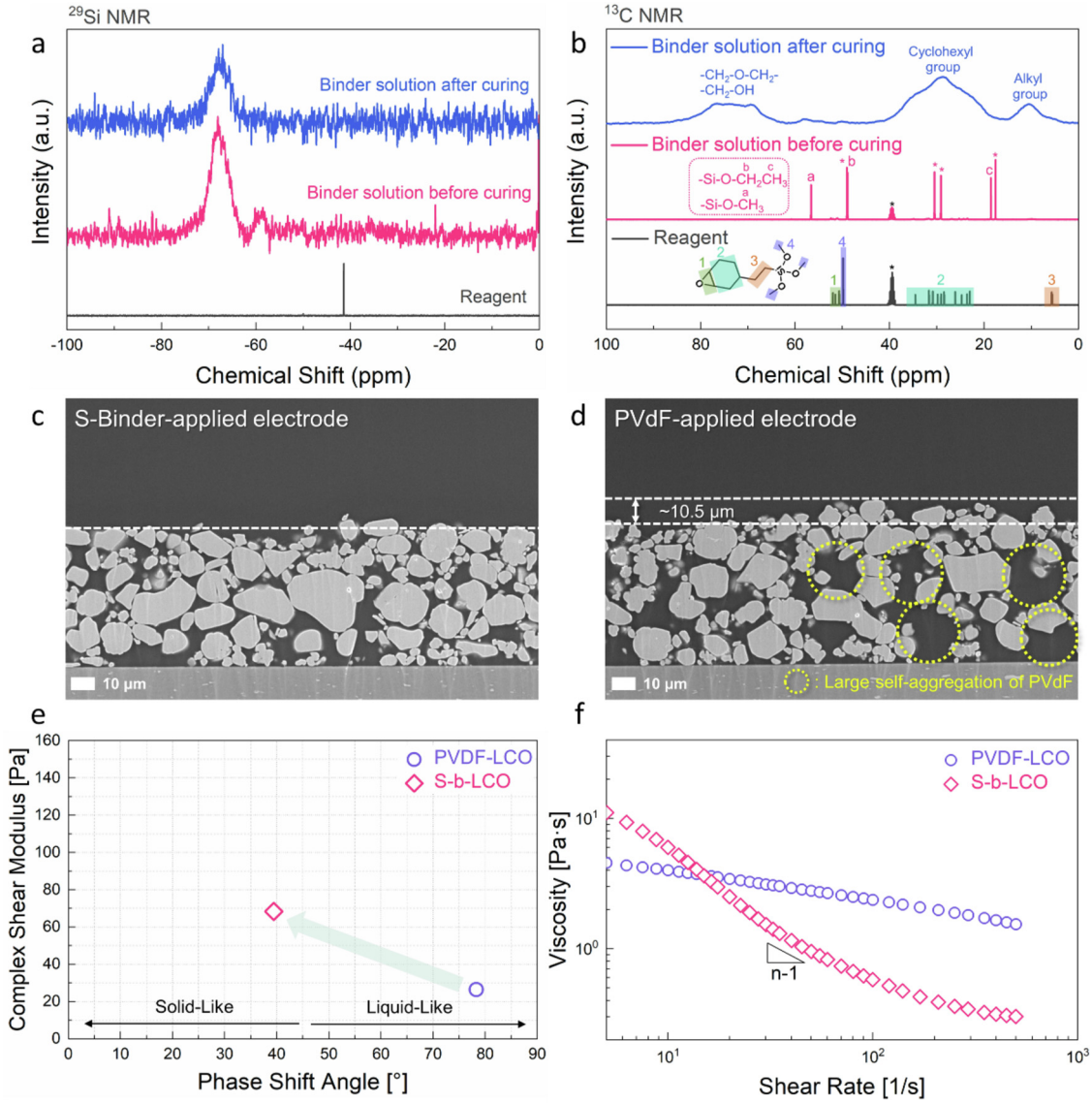

Fig. 3. Characterizations of binders, slurry and electrodes: NMR spectra of (a) ^{29}Si (b) ^{13}C using binder solution before/after curing. Cross-sectional SEM image of electrode surface using (c) S-binder (d) PVDF. (e) Phase angle and complex shear modulus (f) Viscosities of the slurries applied PVDF and S-binder

The merits of S-binder as a novel binder for LIBs are also clearly revealed through comparison of the electrochemical performances of the S-b-LCO and PVDF-LCO electrodes in the voltage range of 3–4.5 V (*vs.* Li^+/Li). As presented in Fig. 4**a–b** and Fig. S7, specific capacities of the S-b-LCO and PVDF-LCO electrodes at 6C (1C = 150 mA g^{-1}) were maintained up to ~73.6% and ~40.4%, respectively, compared with those measured at 0.33C. These results indicate the improved power-capability of $LiCoO_2$ by usage of S-binder instead of PVDF, which is related to smaller charge-transfer resistance of the S-b-LCO (~52.4 Ω) than that of PVDF-LCO (~64.5 Ω) (Fig. 4**c**). Furthermore, to compare direct electrical properties of the S-b-LCO and PVDF-LCO electrodes, we measured resistivities of the active material and the interface between the electrode layer and the current collector (Fig. 4**d**). The total resistance of the electrode is determined by not only the resistivity derived from the environments neighboring active materials but also that attributed to the interface state between the electrode layer and the current collector. The outstanding binder can provide the outstanding adhesion properties with not only the active material but also the current collector. Moreover, it can result in the homogenous coating of the active material with the conductive carbon and the binder. The average resistivity (on the active material) and the interface resistances of the S-b-LCO electrode were ~0.88 Ω•cm and ~0.008 Ω•cm^2, respectively, which are smaller than those of the PVDF-LCO electrode (~1.09 Ω•cm and ~0.0463 Ω•cm^2, respectively). These results indicate that S-binder delivers more outstanding properties as the binder in the LCO-based electrode than PVDF. Average resistivities of the active material and the interface resistances of the S-b-LCO electrode were ~0.88 Ω•cm and ~0.008 Ω•cm^2, respectively, which are smaller than those of the PVDF-LCO electrode (~1.09 Ω•cm and ~0.0463 Ω•cm^2, respectively). These results suggest that the interaction between the current collector and the electrode layer becomes more intense with presence of S-binder, owing to the partially oxidized surface layers of Al foil enabling the interactions between the binder and the current collector, such as Al_2O_3/HO-Si [24]. Moreover, the large resistivity distribution of the PVDF-LCO electrode compared with that of the S-b-LCO electrode implies that S-binder can provide not only homogenous coating of the active material but also outstanding adhesion with the current collector, compared to PVDF. The enhanced power-capability in the S-b-LCO electrode was also confirmed through cyclic voltammetry (CV) and Galvanostatic intermittent titration technique (GITT) analyses. In the CV data (Fig. S8),

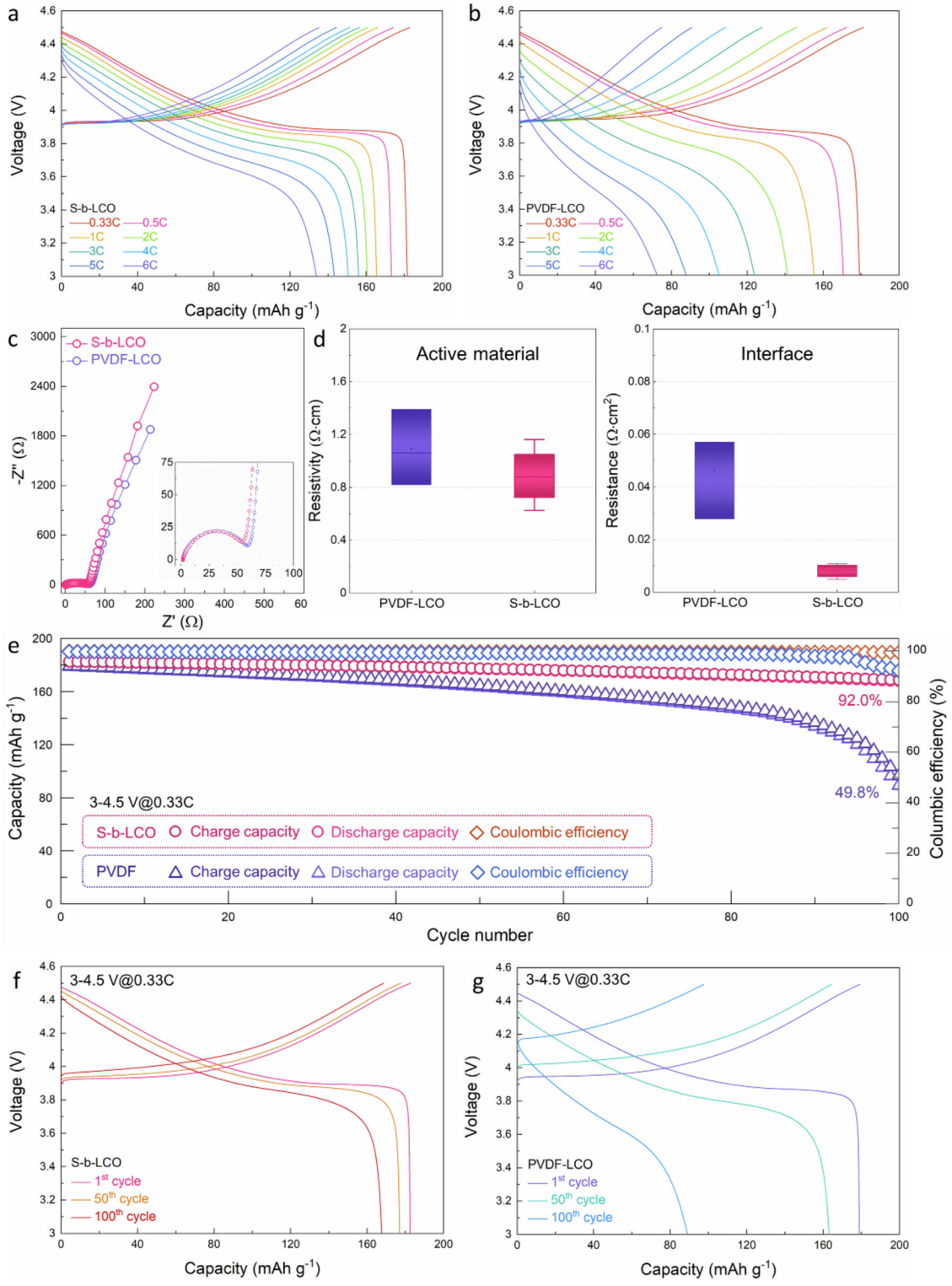

Fig. 4. Characterizations of electrochemical properties of S-b-LCO and PVDF-LCO: Charge/discharge curves at various current density of (a) S-b-LCO (b) PVDF-LCO. (c) Impedance measurements of S-b-LCO and PVDF-LCO (d) Resistivity of the active material and the interface on the S-b-LCO and PVDF-LCO electrode (e) Cycle performances of S-b-LCO and PVDF-LCO. Charge/discharge curves at 1st, 50th and 100th cycles of (f) S-b-LCO (g) PVdF-LCO electrodes

the overpotential of the PVDF-LCO electrode is continuously increased during the prolonged cycling with the voltage range of 3-4.5 V (*vs.* Li^+/Li), whereas the S-b-LCO exhibits the relatively constant overpotential at the same conditions. As presented in Fig. S9, Li-ion diffusion coefficients of the PVDF-LCO electrode based on the GITT analysis are ~5.16×10^{-9} at 0.33C and ~5.45×10^{-10} at 0.5C, which are lower than those of the S-b-LCO (~1.21×10^{-8} at 0.33C and ~5.55×10^{-8} at 0.5C). The enhanced Li-ion diffusion by application of S-binder is consistent with more outstanding power-capability of the S-b-LCO electrode than that of the PVDF-LCO. In addition, Fig. 4**e-g** show that the S-b-LCO electrode exhibited an outstanding capacity retention of ~92.0% compared with the initial capacity after 100 cycles at 0.5C/1C, whereas the ca-

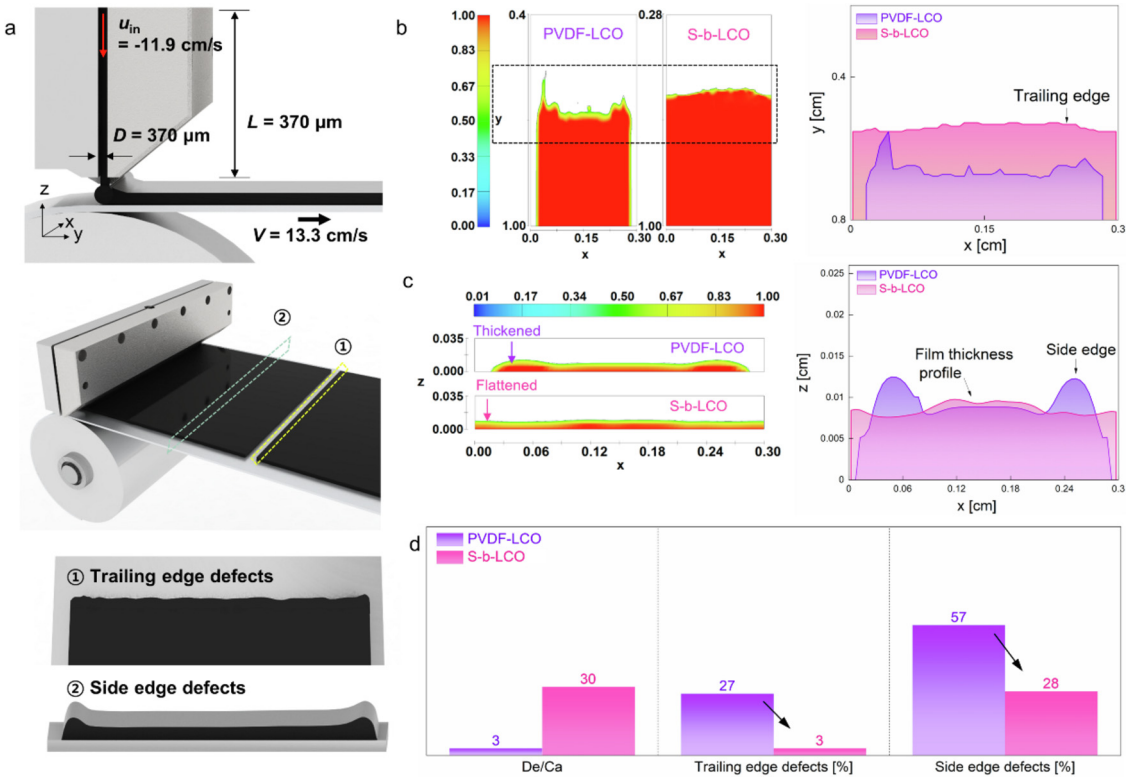

Fig. 5. Coating simulations of S-b-LCO and PVDF-LCO slurries: (a) Schematic image of slot-die coating on the electrode. Comparing (b) trailing edge distributions (c) thickening at the side edge area of S-b-LCO and PVDF-LCO electrodes. (d) Comparing values of De/Ca, trailing edge defects and side edge defects for S-b-LCO and PVDF-LCO

pacity retention of the PVDF-LCO was only ~49.8%. Moreover, Fig. S10 shows that the cycle performance of S-b-LCO electrode for 150 cycles was much better than that of PVDF-LCO electrodes. The comparison of Coulombic efficiency (CE) between S-b-LCO and PVDF-LCO electrodes also indicated the excellence of S-binder compared to PVDF.[25,26] As shown in Fig. 4f, S-b-LCO and PVDF-LCO electrodes exhibited the similar CE of above ~96 % during the initial cycle. After 100 cycles, on the other hand, the CE of S-B-LCO was still retained to above ~99%, which is much larger than that of PVDF-electrode (~92%) (Fig. 4g). These results indicate that S-binder can provide the electrochemical stability even after the prolonged cycling, unlike PVDF. The highly improved cyclability with application of S-binder was also confirmed by *ex-situ* SEM analyses. As shown in Fig. S11, the morphology of the S-b-LCO electrode was well retained after 100 cycles, whereas the surface of the PVDF-LCO electrode was exposed and peeled without covering by the binder.

To evaluate the real application of S-binder for the LIB industry, we performed a simulation of slot-die coating on S-b-LCO and PVDF-LCO slurries. Because of the periodically fed slurry during the intermittent slot-die coating process, qualities of the coating layers are mostly determined by two edge defects: (i) the trailing-edge defect for which the edge lines are curved rather than straight at the transition between the coating being on or off and (ii) the side-edge defect for which the coating layer is thickened at the edge areas [27–29]. For simulation of the slot die, we solved the Navier–Stokes equation in the flow geometry using the volume-of-fluids method (Fig. 5**a**). All the parameters for the simulation are presented in Table S1, and more details are provided in the Experimental section in Supporting Information. As presented in Fig. 5**b**, the uneven trailing-edge distribution is relieved with the addition of S-binder, while the spreading out of the slurry is more severe with PVDF. Fig. 5**c** shows that the thickening at the side-edge areas is observed for the PVDF-based slurry because of the low contact angle between the fluids and substrate. The surface tension and viscoelastic properties of the substrate play important roles during the deposition and drying process, which determines the final film quality [30]. The low contact angle and low surface tension can cause the fluids to draw to the side-edge, resulting in the thicker dry film at edges of the coating. However, the higher surface tension and increased contact angle of the S-binder-added slurries enable avoidance of the deformation of the fluids, resulting in a flatter surface of the electrode (Fig. 5**c**). The dimensionless group De/Ca was evaluated to understand the free surface flows of the slurries. The ratio between the viscous stress μV and surface tension σ can be expressed with the Capillary number $Ca = \mu V/\sigma$ for free surface flows, where μ is the fluid viscosity and V is the fluid velocity. The Deborah number De is the viscoelastic response during the observation time scale and is expressed as $De = \lambda\dot{\gamma}$, where λ and $\dot{\gamma}$ are the relaxation time of fluids and shear rate during processing, respectively. As shown in Fig. 5**d**, De/Ca of the S-binder-based slurry increased up to ten-times larger than that of the PVDF-based slurry, which indicates that the surface tension effect is dramatically increased with usage of S-binder because of the strong associations between Si–O–Si bonding via partial polymerization; this can be favorable for obtaining a more outstanding coating-quality during the drying stage by the full polymerization. In addition, the coating-quality can be quantified with edge defects at the trailing and side regions. The trailing-edge defects are defined by the first y_{min} and last y_{max} break-up position on the stopping line for the y-coordinate (Fig. 5**b**). Again, the side-edge defects are defined by the highest z_{max} and lowest z_{min} position for the z-coordinate (Fig. 5**c**). The two edge failures are significantly reduced by more than half with the S-binder-based slurry compared with the PVDF-based slurry (Fig. 5**d**), which indicates that application of S-binder instead of PVDF enables the highly enhanced electrochemical performances of LIBs.

In this work, we investigated the novel organosilicon-type binder, S-binder for high-performance LIBs. S-binder can adhere the surface of $LiCoO_2$ particles more strongly than PVDF while also possessing

high elasticity and flexibility without the self-aggregation of the binder. Moreover, the viscosity of S-binder can be easily lowered by controlling the shear rate, which results in a uniform thickness of the S-b-LCO electrode. These merits of the S-binder enable much more improved power-capability and stable cycling performance of the S-b-LCO electrode compared with those of the PVDF-LCO electrode. Moreover, it was confirmed that usage of S-binder can decrease the trailing-edge and side-edge defects during the slot-die process compared with the use of PVDF, which indicates that S-binder has great advantages for the mass production of $LiCoO_2$ electrodes compared with PVDF, from the industrial perspective. Furthermore, we estimated that the price of S-binder is below 15 $/kg, which is attributed to typical prices of the raw materials, such as ECTMS (~ 15 $/kg) and TEOS (~5 $/kg). In case of PVDF binder, its commercial price is known to be above 40 $/kg. These contents imply that the organosilicon-type S-binder owns the merit in the industrial point of view. We believe that the proposal of novel binders is one of the key points for efficiently enhancing the electrochemical properties of commercialized LIBs.

4. Conclusion

In this work, we investigated the novel organosilicon-type binder, S-binder for high-performance LIBs. S-binder can adhere the surface of $LiCoO_2$ particles more strongly than PVDF while also possessing high elasticity and flexibility without the self-aggregation of the binder. Moreover, the viscosity of S-binder can be easily lowered by controlling the shear rate, which results in a uniform thickness of the S-b-LCO electrode. These merits of the S-binder enable much more improved power-capability and stable cycling performance of the S-b-LCO electrode compared with those of the PVDF-LCO electrode. Moreover, it was confirmed that usage of S-binder can decrease the trailing-edge and side-edge defects during the slot-die process compared with the use of PVDF, which indicates that S-binder has great advantages for the mass production of $LiCoO_2$ electrodes compared with PVDF, from the industrial perspective. We believe that the proposal of novel binders is one of the key points for efficiently enhancing the electrochemical properties of commercialized LIBs.

Declaration of Competing Interest

The authors declare that they have no known competing financial interests or personal relationships that could have appeared to influence the work reported in this paper.

CRediT authorship contribution statement

Junho Ahn: Validation, Investigation, Resources, Writing – original draft. **Hyeon-Gyun Im:** Validation, Investigation, Writing – review & editing. **Yongseok Lee:** Validation, Visualization, Writing – review & editing. **Dasom Lee:** Visualization, Formal analysis, Methodology. **Hyekyeong Jang:** Formal analysis, Validation. **Youngseok Oh:** Methodology, Investigation. **Kyeongwoon Chung:** Validation. **Teahoon Park:** Visualization. **Moon-Kwang Um:** Conceptualization. **Jin Woo Yi:** Methodology. **Jongsoon Kim:** Project administration, Supervision, Conceptualization, Visualization, Formal analysis, Data curation, Writing – review & editing, Formal analysis. **Dong Jun Kang:** Project administration, Supervision, Conceptualization, Visualization, Formal analysis. **Jung-Keun Yoo:** Project administration, Supervision, Conceptualization, Writing – review & editing, Formal analysis.

Data Availability

Data will be made available on request.

Acknowledgements

This research was supported by the Korea Institute of Materials Science of the Republic of Korea (PNK7670, PNK7980, PNK7330) and the National Research Council of Science and Technology (CAP21041-000). This work was also supported by Korea Electrotechnology Research Institute (21A01015) and National Research Foundation of Korea (NRF-2020M2D8A2070870, NRF-2021M3D1A2049846).

Supplementary materials

Supplementary material associated with this article can be found, in the online version, at doi:10.1016/j.ensm.2022.04.005.

References

[1] G.E. Blomgren, The Development and Future of Lithium Ion Batteries, J. Electrochem. Soc. 164 (1) (2016) A5019–A5025, doi:10.1149/2.0251701jes.
[2] Z.P. Cano, D. Banham, S. Ye, A. Hintennach, J. Lu, M. Fowler, Z. Chen, Batteries and fuel cells for emerging electric vehicle markets, Nature Energy 3 (4) (2018) 279–289, doi:10.1038/s41560-018-0108-1.
[3] K. Moy, S.B. Lee, S. Harris, S. Onori, Design and validation of synthetic duty cycles for grid energy storage dispatch using lithium-ion batteries, Advances in Applied Energy 4 (2021) 100065, doi:10.1016/j.adapen.2021.100065.
[4] W. He, W. Guo, H. Wu, L. Lin, Q. Liu, X. Han, Q. Xie, P. Liu, H. Zheng, L. Wang, X. Yu, D.-L. Peng, Challenges and Recent Advances in High Capacity Li-Rich Cathode Materials for High Energy Density Lithium-Ion Batteries, Adv. Mater. (2021) 2005937 n/a (n/a), doi:10.1002/adma.202005937.
[5] H. Cheng, J.G. Shapter, Y. Li, G. Gao, Recent progress of advanced anode materials of lithium-ion batteries, Journal of Energy Chemistry 57 (2021) 451–468, doi:10.1016/j.jechem.2020.08.056.
[6] K. Wang, J. Wan, Y. Xiang, J. Zhu, Q. Leng, M. Wang, L. Xu, Y. Yang, Recent advances and historical developments of high voltage lithium cobalt oxide materials for rechargeable Li-ion batteries, J. Power Sources 460 (2020) 228062, doi:10.1016/j.jpowsour.2020.228062.
[7] C. Sun, X. Liao, F. Xia, Y. Zhao, L. Zhang, S. Mu, S. Shi, Y. Li, H. Peng, G. Van Tendeloo, K. Zhao, J. Wu, High-Voltage Cycling Induced Thermal Vulnerability in LiCoO2 Cathode: Cation Loss and Oxygen Release Driven by Oxygen Vacancy Migration, ACS Nano 14 (5) (2020) 6181–6190, doi:10.1021/acsnano.0c02237.
[8] J. Li, C. Lin, M. Weng, Y. Qiu, P. Chen, K. Yang, W. Huang, Y. Hong, J. Li, M. Zhang, C. Dong, W. Zhao, Z. Xu, X. Wang, K. Xu, J. Sun, F. Pan, Structural origin of the high-voltage instability of lithium cobalt oxide, Nat. Nanotechnol. 16 (5) (2021) 599–605, doi:10.1038/s41565-021-00855-x.
[9] X. Yang, M. Lin, G. Zheng, J. Wu, X. Wang, F. Ren, W. Zhang, Y. Liao, W. Zhao, Z. Zhang, N. Xu, W. Yang, Y. Yang, Enabling Stable High-Voltage $LiCoO_2$ Operation by Using Synergetic Interfacial Modification Strategy, Adv. Funct. Mater. 30 (43) (2020) 2004664, doi:10.1002/adfm.202004664.
[10] Q. Liu, X. Su, D. Lei, Y. Qin, J. Wen, F. Guo, Y.A. Wu, Y. Rong, R. Kou, X. Xiao, F. Aguesse, J. Bareño, Y. Ren, W. Lu, Y. Li, Approaching the capacitylimit of lithium cobalt oxide in lithium ion batteries via lanthanum and aluminium doping, Nature Energy 3 (11) (2018) 936–943, doi:10.1038/s41560-018-0180-6.
[11] J. Qian, L. Liu, J. Yang, S. Li, X. Wang, H.L. Zhuang, Y. Lu, Electrochemical surface passivation of $LiCoO_2$ particles at ultrahigh voltage and its applications in lithium-based batteries, Nat. Commun. 9 (1) (2018) 4918, doi:10.1038/s41467-018-07296-6.
[12] J.-N. Zhang, Q. Li, C. Ouyang, X. Yu, M. Ge, X. Huang, E. Hu, C. Ma, S. Li, R. Xiao, W. Yang, Y. Chu, Y. Liu, H. Yu, X.-Q. Yang, X. Huang, L. Chen, H. Li, Trace doping of multiple elements enables stable battery cycling of $LiCoO_2$ at 4.6 V, Nature Energy 4 (7) (2019) 594–603, doi:10.1038/s41560-019-0409-z.
[13] F. Zou, A. Manthiram, A Review of the Design of Advanced Binders for High-Performance Batteries, Adv. Energy Mater. 10 (45) (2020) 2002508, doi:10.1002/aenm.202002508.
[14] Y. Shi, X. Zhou, G. Yu, Material and Structural Design of Novel Binder Systems for High-Energy, High-Power Lithium-Ion Batteries, Acc. Chem. Res. 50 (11) (2017) 2642–2652, doi:10.1021/acs.accounts.7b00402.
[15] J. Xu, S.-L. Chou, Q.-f. Gu, H.-K. Liu, S.-X. Dou, The effect of different binders on electrochemical properties of $LiNi_{1/3}Mn_{1/3}Co_{1/3}O_2$ cathode material in lithium ion batteries, J. Power Sources 225 (2013) 172–178, doi:10.1016/j.jpowsour.2012.10.033.
[16] H. Chen, M. Ling, L. Hencz, H.Y. Ling, G. Li, Z. Lin, G. Liu, S. Zhang, Exploring Chemical, Mechanical, and Electrical Functionalities of Binders for Advanced Energy-Storage Devices, Chem. Rev. 118 (18) (2018) 8936–8982, doi:10.1021/acs.chemrev.8b00241.
[17] Y.-W. Lim, J. Jin, B.-S. Bae, Optically Transparent Multiscale Composite Films for Flexible and Wearable Electronics, Adv. Mater. 32 (2020) 1907143 http://doi.org/10.1002/adma.201907143.
[18] H.-G. Im, G.U. Park, H.Y. Park, J. Jin, D.J. Kang, A robust transparent protective hard-coating material using physicochemically-incorporated silica nanoparticles and organosiloxanes, Prog. Org. Coat. 105 (2017) 330–335, doi:10.1016/j.porgcoat.2017.02.004.

[19] R. Ciriminna, A. Fidalgo, V. Pandarus, F. Béland, L.M. Ilharco, M. Pagliaro, The Sol–Gel Route to Advanced Silica-Based Materials and Recent Applications, Chem. Rev. 113 (8) (2013) 6592–6620, doi:10.1021/cr300399c.
[20] J. Jang, H.-G. Im, D. Lim, B.-S. Bae, Preparation of high-performance transparent glass-fiber reinforced composites based on refractive index-tunable epoxy-functionalized siloxane hybrid matrix, Compos. Sci. Technol. 201 (2021) 108527, doi:10.1016/j.compscitech.2020.108527.
[21] B. Chang, J. Kim, Y. Cho, I. Hwang, M.S. Jung, K. Char, K.T. Lee, K.J. Kim, J.W. Choi, Highly Elastic Binder for Improved Cyclability of Nickel-Rich Layered Cathode Materials in Lithium-Ion Batteries, Adv. Energy Mater. 10 (29) (2020) 2001069, doi:10.1002/aenm.202001069.
[22] G. Paul, C. Bisio, I. Braschi, M. Cossi, G. Gatti, E. Gianotti, L. Marchese, Combined solid-state NMR, FT-IR and computational studies on layered and porous materials, Chem. Soc. Rev. 47 (15) (2018) 5684–5739, doi:10.1039/C7CS00358Gd.
[23] J.-K. Yoo, Y. Oh, T. Park, K. Lee, M.-K. Um, J.-W. Yi, Optimization of Carbon Nanotubes as Conductive Additives for High-Energy-Density Electrodes for Lithium-Ion Batteries, Energy Technology 7 (5) (2018), doi:10.1002/ente.20180084.
[24] J. Yang, P. Li, F. Zhong, X. Feng, W. Chen, X. Ai, H. Yang, D. Xia, Y. Cao, Suppressing Voltage Fading of Li-Rich Oxide Cathode via Building a Well-Protected and Partially-Protonated Surface by Polyacrylic Acid Binder for Cycle-Stable Li-Ion Batteries, Adv. Energy Mater. 10 (15) (2020) 1904264, doi:10.1002/aenm.201904264.
[25] H. Li, Practical Evaluation of Li-Ion Batteries, Joule 3 (4) (2019) 908–919, doi:10.1016/j.joule.2019.03.028.
[26] Z. Lin, T. Liu, X. Ai, C. Liang, Aligning academia and industry for unified battery performance metrics, Nat. Commun. 9 (2018) 5262, doi:10.1038/s41467-018-07599-8.
[27] M. Schmitt, P. Scharfer, W. Schabel, Slot die coating of lithium-ion battery electrodes: investigations on edge effect issues for stripe and pattern coatings, J. Coat. Technol. Res. 11 (1) (2014) 57–63, doi:10.1007/s11998-013-9498-y.
[28] P. Tan, S. Diao, T. Huang, Z. Yang, H. Zhou, Y. Zhang, Mechanism and Control of the Trailing Edge in Intermittent Slot Die Coating, Ind. Eng. Chem. Res. 59 (35) (2020) 15758–15767, doi:10.1021/acs.iecr.0c02743.
[29] R. Diehm, H. Weinmann, J. Kumberg, M. Schmitt, J. Fleischer, P. Scharfer, W. Schabel, Edge Formation in High-Speed Intermittent Slot-Die Coating of Disruptively Stacked Thick Battery Electrodes, Energy Technology 8 (2) (2020) 1900137, doi:10.1002/ente.201900137.
[30] N. Aggarwal, K. Sarkar, Effects of matrix viscoelasticity on viscous and viscoelastic drop deformation in a shear flow, J. Fluid Mech. 601 (2008) 63–84, doi:10.1017/S0022112008000451.